Notes on HARDI data preprocessing

Scott Trinkle

Last edited: January 25, 2019

1 Introduction

This report describes the steps in preprocessing the HARDI mouse data. Namely, it details the application of a denoising algorithm and the spatial registration of the data acquired with different diffusion weightings.

2 Denoising

The denoising algorithm comes from a paper by Veraart *et al* [1], and is implemented in the MRtrix3 software package, written by the Tournier group.

2.1 Denoising method summary

Consider a real-valued, redundant dMRI data matrix $\boldsymbol{X}$, with M rows representing different diffusion-weighted measurements and N columns representing voxels within a local neighborhood. The assumption of data "redundancy" amounts to the assumption that the data can be synthesized by a small number, $P \ll \min(M, N)$ of principal components. Veraart shows in another paper [2] that the oversampling of q-space in dMRI leads to sufficient redundancy.

Principal components of $\boldsymbol{X}$ can be derived via singular value decomposition of $\boldsymbol{X}$:

$$\boldsymbol{X} = \sqrt{N}\boldsymbol{U}\boldsymbol{\Lambda}\boldsymbol{V}^T, \tag{1}$$

where the singular value, $\Lambda_{ii}^2 = \lambda_i$ is the ith eigenvalue of the $M \times M$ matrix:

$$\boldsymbol{\Sigma} = \frac{1}{N}\boldsymbol{X}\boldsymbol{X}^T. \tag{2}$$

A note on notation: the paper assumes $M < N$ for the purposes of the derivation, though that choice is arbitrary, and is obviously not the case for our data.

Noise will generally make all M eigenvalues of $\boldsymbol{\Sigma}$ nonzero. In agreement with an asymptotic universal law resulting from random matrix theory for noisy covariance matrices, the $\tilde{M} = M - P$ smallest nonzero eigenvalues are described by the Marchenko-Pastur (MP) distribution if the noise level is constant among all elements of $\boldsymbol{X}$ [3]:

$$p(\lambda, \sigma, \gamma) = \begin{cases} \frac{\sqrt{(\lambda_+ - \lambda)(\lambda - \lambda_-)}}{2\pi\gamma\lambda\sigma^2} & \text{if } \lambda_- \leq \lambda \leq \lambda_+ \\ 0 & \text{otherwise,} \end{cases} \tag{3}$$

where

$$\lambda_\pm = \sigma^2(1 \pm \sqrt{\gamma})^2, \tag{4}$$

$$\gamma = \tilde{M}/N, \tag{5}$$

and σ^2 is the noise variance.

The distribution edge λ_+ distinguishes between noise- and signal-carrying principal components. The matrix can thus be denoised by nullifying all $\lambda \leq \lambda_+$, setting $\boldsymbol{\Lambda} \rightarrow \tilde{\boldsymbol{\Lambda}}$ accordingly, and reconstructing the matrix from the SVD:

$$\hat{\boldsymbol{X}} = \sqrt{N}\boldsymbol{U}\tilde{\boldsymbol{\Lambda}}\boldsymbol{V}^T. \tag{6}$$

This method **assumes the noise level to be constant and uncorrelated within the local neighborhood and across the dMRI measurements.** We need to think about whether these assumptions hold given the time duration of our scan.

The rest of the paper is spent deriving and testing an algorithm for simultaneously estimating the noise level σ and the number of significant signal components P. This algorithm is implemented in MRtrix3.

2.2 Implementation

The only tunable parameter available from the MRtrix3 implementation is N: the size of the local sliding window used to define each $\boldsymbol{X}$. Veraart *et al* suggest choosing $N > M$, but note: "in case of spatially varying noise, it might be beneficial to select a sliding window with $N \gtrsim M$." To test, I denoised the data with windows of size $5 \times 5 \times 5$ ($N = 125$), $7 \times 7 \times 7$ ($N = 343$) and $9 \times 9 \times 9$ ($N = 729$). Note that $M = 160$ for our data (16 b_0 volumes and 144 diffusion-weighted volumes). Sample denoised slices from a b_0 and a diffusion-weighted image (DWI) are shown in Figure 1 below.

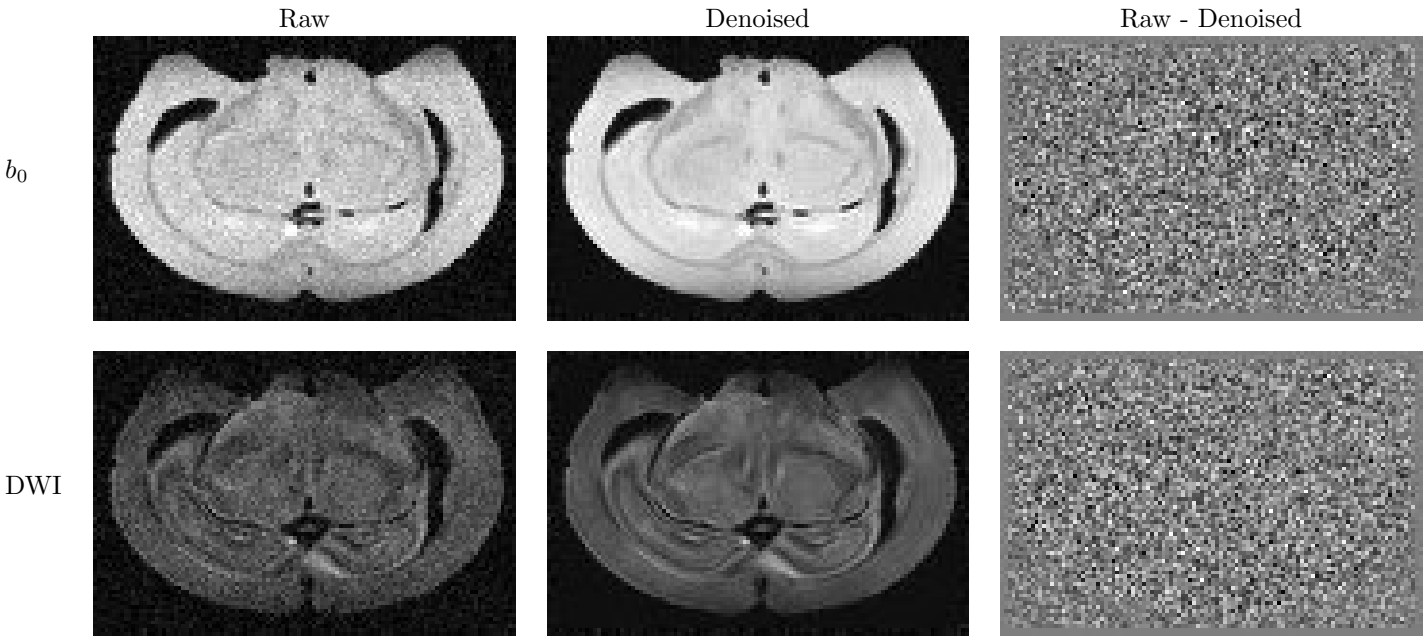

Figure 1: Top and bottom demonstrate denoising of a b_0 and diffusion weighted volume, respectively. Left, center and right are the raw, denoised, and subtracted images, respectively. Note the lack of identifiable anatomical structure in the subtracted images. These images were processed using a $7 \times 7 \times 7$ sliding window.

As a first-pass check, it is promising that no anatomical structure is visible in the subtracted images for either the b_0 or diffusion-weighted images. These sample images were calculated using a $7 \times 7 \times 7$ sliding window; there was also no structure visible for the other widths.

3 Registration

Minor drifts in the B_0 field across the 16-day scan cause slight, linear position shifts across the different DWI. The data were acquired with 1 b_0 image after every 9 DWI, for a total of 16 b_0's and 144 DWIs. The registration strategy was to first register the 16 b_0's, average them to generate a mean $\bar{b}_0$, then register the 144 DWIs to $\bar{b}_0$. All registrations were affine, calculated with the FLIRT [4, 5] tool in FSL (this was based on Sean's recommendation).

3.1 b_0 registration

The b_0's were registered using a correlation-based cost function (appropriate since we expect the same contrast for each b_0). I investigated two FLIRT parameters to modify to tune the registration: affine degrees of freedom, and voxel-weighting. The data denoised with a $7 \times 7 \times 7$ window width were used to determine optimal parameters.

All b_0's were registered to the 8th volume. Of note: there are certain structures that appear in the first 4 b_0 volumes that do not appear in the later ones. This is demonstrated in Figure 2. It is unclear to me why this happened, I need to discuss it further with Sean.

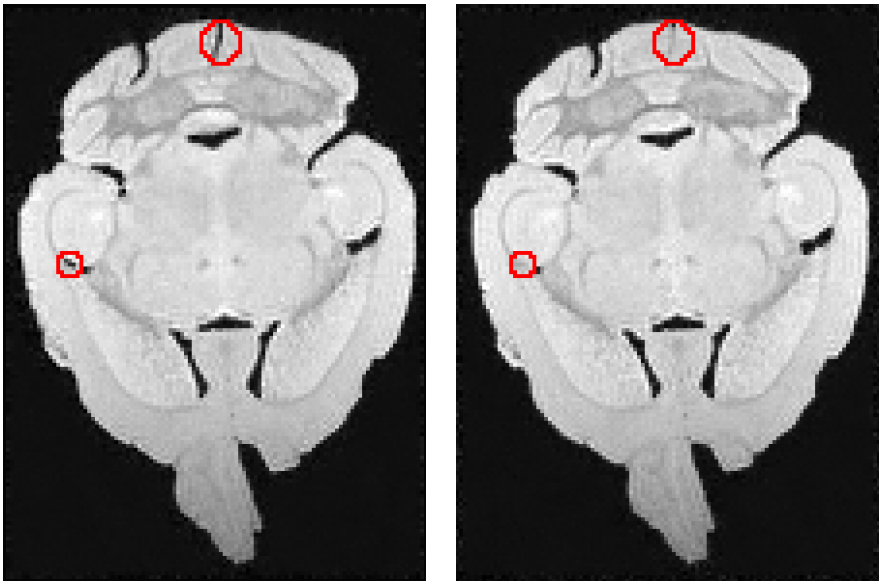

b_0 #0 b_0 #8

Figure 2: Evidence of structures in earlier b_0 volumes that does not appear in later volumes.

Figure 3 shows the performance of the registrations as a function of affine degrees of freedom. The x-axis shows the b_0 volume number, and the y-axis shows the pearson correlation coefficient between the voxels of the registered volume and the reference volume (#8). The dotted lines indicate the average correlation coefficient for each curve. We see that the additional structures in the earlier volumes negatively impact the relative registration accuracy. Overall, using all 12 degrees of freedom had the best performance.

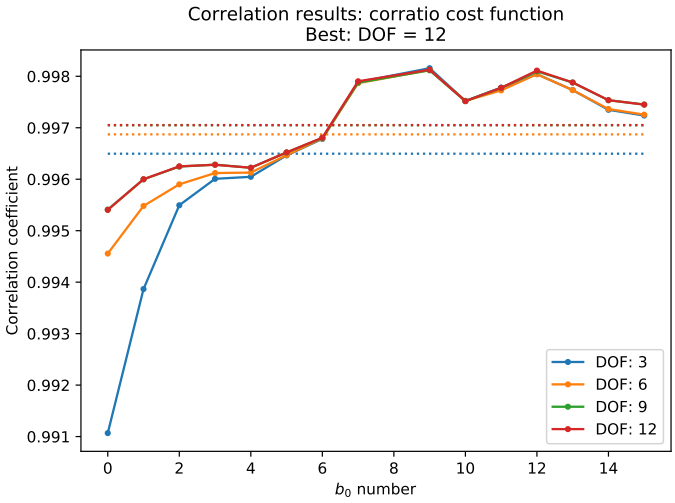

Figure 3: Selection of optimal b_0 DOF. Note the worse performance in the earlier volumes with the additional structures

FLIRT also allows you to input an image to use as weights for each voxel in the optimization. Using 12 degrees of freedom, I experimented with using the reference image (#8) and the first image (#0) as voxel weights. The reasoning was that both images would weight object voxels higher than background, while the #0 image would place a lower weight on the additional structures, since they have lower intensity. Figure 4 shows the results of these two weighting schemes compared to an non-weighted registration.

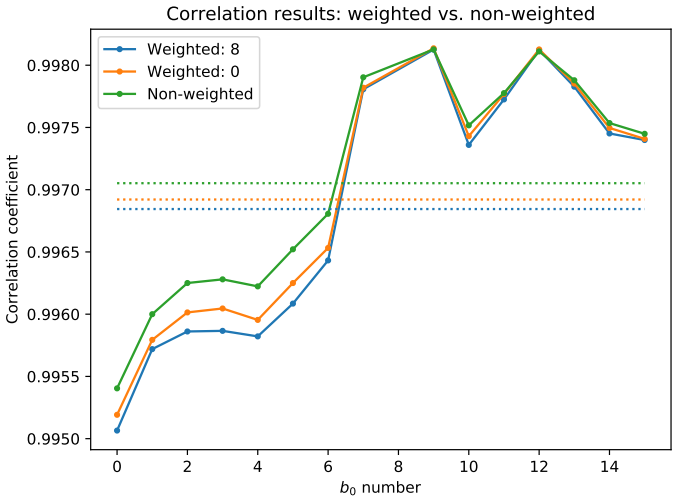

Figure 4: Selection of b_0 weighting parameters.

The unweighted registration performed better for all individual volumes. Accordingly, I decided to use an unweighted, 12-DOF affine registration for all b_0 volumes.

3.2 DWI Registration

Since the DWIs necessarily have different contrast for the same structures, they were registered using a mutual information cost function. The strategy was to average the registered b_0 volumes into a single $\bar{b}_0$, then use that as a reference for the DW volumes. Again, I investigated affine degrees of freedom and voxel weighting to tune the registration. Figure 5 shows the mutual information results for varying degrees of freedom and voxel weightings. For this study, voxel weighting was done with $\bar{b}_0$.

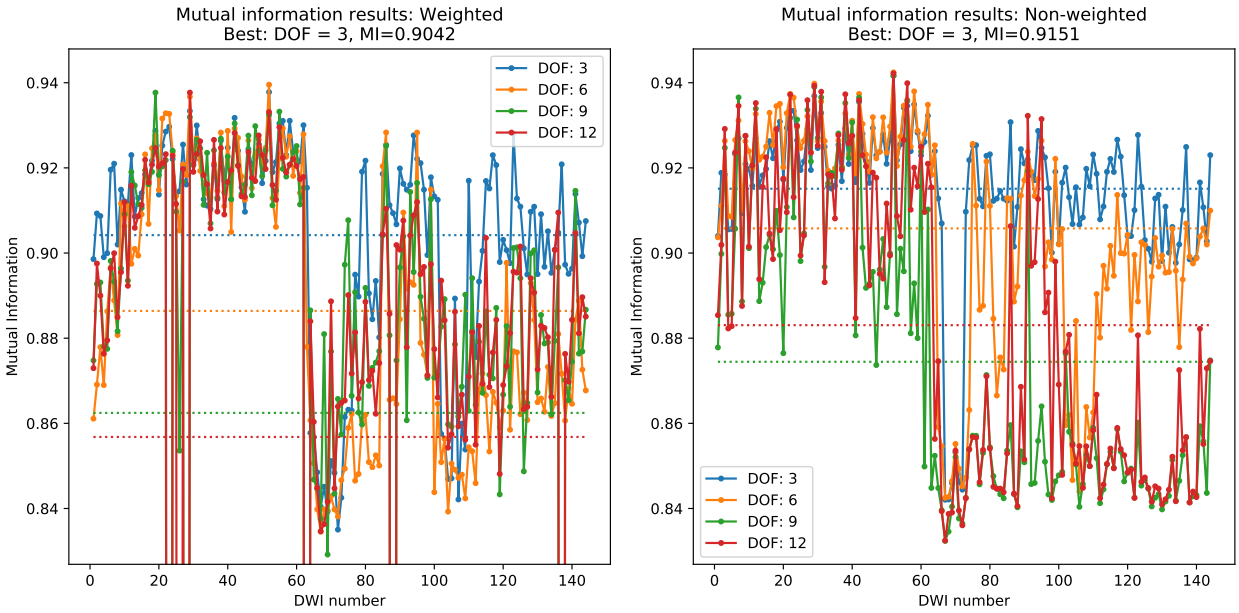

Figure 5: Diffusion-weighted image registration results.

In general, using 3 degrees of freedom (equivalent to a rigid translation) performed the best. Voxel weighting generally degraded performance; using 3 degrees of freedom with no voxel weighting resulted in the best registration overall.

4 Conclusion

The raw data, as well as the data denoised with the three different sliding window widths were registered using the strategy and optimal parameters described above. The next report will detail the effect of denoising on ODF reconstruction, as well as exploring ODF sensitivity to sliding window width.

References

[1] J. Veraart, D. S. Novikov, D. Christiaens, B. Ades-aron, J. Sijbers, and E. Fieremans, "Denoising of diffusion MRI using random matrix theory," *NeuroImage*, vol. 142, pp. 394–406, nov 2016.

[2] J. Veraart, E. Fieremans, and D. S. Novikov, "Diffusion MRI noise mapping using random matrix theory," *Magnetic Resonance in Medicine*, vol. 76, pp. 1582–1593, nov 2016.

[3] V. Marchenko and L. Pastur, "Distribution of eigenvalues for some sets of random matrices," *Matematicheskii Sbornik*, vol. 114, no. 4, pp. 507–536, 1967.

[4] M. Jenkinson and S. Smith, "A global optimisation method for robust affine registration of brain images.," *Medical image analysis*, vol. 5, pp. 143–56, jun 2001.

[5] M. Jenkinson, P. Bannister, M. Brady, and S. Smith, "Improved optimization for the robust and accurate linear registration and motion correction of brain images.," *NeuroImage*, vol. 17, pp. 825–41, oct 2002.